Kashf Journal of Multidisciplinary Research
Vol:03 – Issue 03 (2026)
P-ISSN: 3007-1992 E-ISSN: 3007-200X
https://kjmr.com.pk

HYBRID CUBIC B-SPLINE COLLOCATION METHOD FOR THE NUMERICAL SOLUTION OF THE ALLEN–CAHN EQUATION

***Roohi Aaysha[1], Muhammad Amin[2], Iqra safdar[3], Muhammad Usama[4]**

*[1, 2, 3, 4]Faculty of Sciences, The Superior University Lahore, Pakistan.

[*]***Corresponding Author:***(roohiayesha49@gmail.com)

DOI:(*https://doi.org/10.71146/kjmr861*)

Article Info

Abstract

Allen Cahn equation is a famous nonlinear partial differential equation which is applied to characterize phase separation and motion of interfaces in multi-component systems. It is also used in materials science, fluid dynamics and image processing. In this article, the extended cubic B-spline functions along with finite difference scheme is suggested for the numerical treatment of time fractional Allen-Cahn equation. The approach employs the smoothness and local support of cubic B-spline basis functions. The spatial discretization in the proposed scheme is done using extended cubic B-splines. Whereas Caputo's formula is used for temporal discretization. Numerical experiments are given to investigate the performance of the method. The findings reveal that the scheme is very accurate, convergent and has less numerical error. The extended cubic B-spline method is therefore a safe and effective method to use in solving nonlinear reaction-diffusion equations like the Allen-Cahn equation. α α

Keywords: *Allen–Cahn equation; Extended cubic B-spline Method; Numerical solution; Finite difference method; Stability and convergence analysis.*

1. Introduction

Allen Cahn equation is a famous nonlinear reaction diffusion partial differential equation that was first proposed to model the phase separation and antiphase boundary motion in multi-component alloy systems [1]. It is a mathematical description of the time dynamics of a parameter that characterizes the various phases of a material and has found applications in materials science, fluid mechanics and image processing because it can be used to describe interface dynamics and pattern formation [2].

The one-dimensional Allen–Cahn equation is commonly written as

$$\frac{\partial^{\alpha} q}{\partial t^{\alpha}} - \frac{\partial^2 q}{\partial p^2} + q^3 - q(p,t) = v(p,t) \quad \mathrm{p} \in [\mathrm{a},\mathrm{b}], \quad \mathrm{t} \in [0,\mathrm{T}], \tag{1}$$

Here, $q(\mathrm{p},t)$ is the unknown function, ε denotes small positive constant controlling interface width and $[a,b]$ represents the spatial domain.

With the initial condition that specifies the state of the system at time $t = 0$:

$$\mathrm{q}(\mathrm{p},0) = \varphi(\mathrm{p}), \qquad a \le p \le b\,. \tag{2}$$

And the boundary conditions:

$$q(a,t) = \psi_1(t), \quad q(\mathrm{b},t) = \psi_2(t), \tag{3}$$

Where $\alpha \in (0, 1)$ and $v(\mathrm{p}, \mathrm{t})$ is the source term. Ψ and φ are smooth and continuous functions with first order derivatives.

Owing to this high nonlinearity and the existence of sharp interfaces, it is hard to find analytical solutions that are correct in all but very special cases [3].

Consequently, many numerical methods have been developed to approximate its solution. This has led to numerous mathematical techniques being devised to estimate its solution. Initial attempts were directed at finite difference and gradient schemes in order to provide stable time evolution. Later, there were the introduction of finiteness element approximations to enhance spatial accuracy and deal with complex boundary conditions [4]. The use of spectral and fourier based techniques has also been used because of high accuracy in smooth solutions.

The spline-based methods have been popular due to their smoothness, local support and good approximation qualities. Numerical analysis literature has an extensive theory and practical construction of spline functions [5]. Cubic B-splines offer continuous second-order derivatives and flexible curve fitting, so they can be used in solving differential equations. Cubic B-spline collocation has been effectively used with nonlinear diffusion equations and reaction-diffusion equations

that exhibit satisfactory accuracy and convergence [6]. Stable and higher-order time-accurate phase-field models schemes have more recently been proposed in order to increase efficiency and long-time stability [7]. The AllenCahn model has also been studied using discontinuous Galer kin and sophisticated numerical frameworks to enhance reliability [8].

Inspired by this advancements, the current research paper suggests an extended cubic B-spline algorithm to solve the Allen-Cahn equation[9]. The scheme is a combination of cubic B-spline spatial discretization, a time integration scheme based on finite difference, and a linearization of the nonlinear term. The goal is to obtain greater accuracy, stability and computational efficiency. The method is analyzed in terms of stability and convergence properties and numerical experiments are conducted to determine its efficacy. The findings validate that the suggested method has the correct solutions and is capable of capturing the dynamics of the interface in nonlinear reaction diffusion equation [11]. First proposed in 1979, the Allen-Cahn equation is a basic nonlinear reaction-diffusion equation, commonly employed to model phase separation and interface motion in multi-component systems. Analytical solutions are typically challenging to find, especially when problems are time-dependent and of a higher dimension, due to its nonlinear form and stiffness. Consequently, numerical techniques are important in providing approximate solutions. Both numerical schemes are stressed in recent works where the AllenCahn equation is solved with stable and efficient numerical schemes [12].

Classical numerical methods including the finite difference methods (FDM) and finite element methods (FEM) have been widely used. The use of finite difference is the method of choice because it is simple and easy to implement especially in cases where the implicit or semi-implicit schemes are employed to deal with stiffness. The efficient techniques of finite differentiation have been created to enhance computational stability and efficiency [13]. Conversely, finite element approaches offer greater flexibility when dealing with complicated geometries and boundary conditions, and high-order schemes can model sharp interface dynamics [14]. These classical approaches could however need very fine discretization in the case of nonlinear problems. Spline based numerical methods have become a good alternative because they are higher order in continuity and smoothness. Specifically, cubic B-spline methods have been used to offer good solutions to nonlinear partial differential equations including AllenCahn equation. Recent research shows that spline-based methods are accurate and efficient [15].

Extended cubic B-spline methods further enhance performance by combining classical spline interpolation with cubic B-spline basis functions. This hybrid structure improves convergence, stability, and local control of the solution [16]. It has been reported that hybrid spline schemes outperform standard spline methods by reducing numerical oscillations and improving accuracy [17]. Furthermore, hybrid schemes on complex domains present good numerical properties [18].

Recent research has been interested in combining spline-based methods with contemporary numerical methods. Meshless techniques, adaptive time-stepping schemes and new numerical structures have enhanced efficiency for higher-dimensional problems [19]. Additionally, new methods such as physics-informed neural networks offer new insights into the solution of nonlinear partial differential equations [20].

In conclusion, extended cubic B-spline schemes offer a robust and effective approach for solving the Allen-Cahn equation. They combine accuracy, stability and efficiency, making them ideal for phase-field simulations [21].

2. Preliminaries

Let $q(p,t)$ be a smooth enough function in the spatial domain $[a,b]$. The solution of the Allen-Cahn equation by Extended cubic B-spline functions is achieved by dividing the spatial interval into subintervals of equal length and using the spline basis functions to approximate the solution.

The interval $[a,b]$ is divided into N equal subintervals.

The spatial domain $[a,b]$ is discretized into N equal subintervals with a uniform grid width

$$h = \frac{b-a}{N}$$

The grid points are given by

$$xi = a + ih, \qquad i = 0,1,2,\ldots,N.$$

The numerical approximation $U(x,t)$ is defined as a linear combination of Extended cubic B-spline basis functions in the following form

$$U(x,t) = \sum_{i=-1}^{N+1} \delta_i(t) B_i(x),$$

Where $B_i(x)$ are the Extended cubic B-spline basis functions and $\delta_i(t)$ are time-dependent unknown parameters that need to be determined [22].

Using the properties of spline functions, the function value and its derivatives at the grid points can be expressed in terms of the spline parameters. At the grid point x_i the approximate solution can be written as

$$U_i = \delta_{i-1} + 4\delta_i + \delta_{i+1}$$

Similarly, the second spatial derivative required in the Allen–Cahn equation is approximated as

$$Uxx = \frac{6}{h^2}(\delta_{i-1} - 2\delta_i + \delta_{i+1}).$$

$$D_t^a u(x,t) = \varepsilon^2 \frac{\partial^2 u(x,t)}{\partial x^2} + u(x,t) - u^3(x,t)$$

Caputo -Fabrizio Fractional operator is

$$D_t^a u(x,t) = \frac{M(\alpha)}{1-\alpha}\int_0^t \frac{\partial u(x,t)}{\partial \tau}\exp\left[-\frac{\alpha}{1-\alpha}(t-\tau)\right]d\tau$$

2.1. Basis functions

Extended cubic B-spline ExCBS is the extension of the cubic B-spline with an additional free parameter σ. The free parameter is introduced in basis functions to allow changes to the generated curves[23].

The basis function of Hybrid CBS with four degrees is defined as follows

$$C_j(p,\sigma) = \frac{1}{24h^4}\begin{cases} 4h(1-\sigma)\left(p-p_j\right)^3 + 3\sigma\left(p-p_j\right)^4, p\in\left[p_j, p_{j+1}\right), \\ (4-\sigma)h^4 + 12h^3\left(p-p_{j+1}\right) + 6h^2(2+\sigma)\left(p-p_{j+1}\right)^2, \\ -12h\left(p-p_{j+1}\right)^3 - 3\sigma\left(p-p_{j+1}\right)^4, p\in\left[p_{j+1}, p_{j+2}\right), \\ (4-\sigma)h^4 + 12h^3\left(p_{j+3}-p\right) + 6h^2(2+\sigma)\left(p_{j+3}-p\right)^2 \\ -12h\left(p_{j+3}-p\right)^3 - 3\sigma\left(p_{j+3}-p\right)^4, p\in\left[p_{j+2}, p_{j+3}\right), \\ 4h(1-\sigma)\left(p_{j+4}-p\right)^3 + 3\sigma\left(p_{j+4}-p\right)^4, p\in\left[p_{j+3}, p_{j+4}\right), \\ 0, otherwise, \end{cases} \quad (4)$$

Where p is the variable and $\sigma \in R$. For $-8 \le \sigma \le 1$, the Hybrid CBS functions possess the Various properties of B-spline, such as the convex hull property, symmetry and geometric Invariance[24]. If we substitute $\sigma = 0$, the basis function of extended spline will reduce to CBS Function. Now, consider the Hybrid CBS approximation for $q(p,t)$ to be $Q(p,t)$ as

$$Q(p,t) = \sum_{k=-1}^{n+1} \eta_k^m(t) C_k(p,\sigma), \quad (5)$$

Where $\eta_k^m(t)$ are the control points which are computed at each time level and $C_k(p,\sigma)$ are the Hybrid CBS functions? Due to the local support property of basis function, that is $C_k(p,\sigma)$ are non-zero in $\left[p_j, p_j+4\right)$, it contains only three non-zero basis functions, namely $C_{k-1}(p,\sigma), C_k(p,\sigma)$ and $C_{k+1}(p,\sigma)$ for the evaluation at each p_j.

The coefficients of Hybrid CBS functions and their derivatives at knots p_j are:

$$C(p_j,\sigma)=\begin{cases}\dfrac{8+\sigma}{12}, if k-j=0\\ \dfrac{4-\sigma}{24}, if k-j=\pm 1,\\ 0, otherwise,\end{cases} \tag{6}$$

$$C^{'}(p_j,\sigma)=\begin{cases}0, if\ \ k-j=0\\ \pm\dfrac{1}{2h}, if\ \ k-j=\pm 1\\ 0, Otherwise\end{cases} \tag{7}$$

$$C''\left(p_j,\sigma\right)=\begin{cases}-\dfrac{2+\sigma}{h^2}, if k-j=0\\ \dfrac{2+\sigma}{h^2}, if k-j=\pm 1\\ 0, Otherwise\end{cases} \tag{8}$$

Formulation of New Approximation for $Q''\left(p,t\right)$

To find new Hybrid CBS function $Q''\left(p,t\right)$ for second derivative $q''\left(p_j\right)$

$$C_0=\frac{1}{24h^2}\left(2\left(14-\sigma\right)\eta_{-1}+3\left(3\sigma-22\right)\eta_0+8\left(7-2\sigma\right)\eta_1+14\left(\sigma-2\right)\eta_2+6\left(2-\sigma\right)\eta_3+\left(\sigma-2\right)\eta_4\right) \tag{9}$$

$$C_j=\frac{1}{24h^2}\left(\left(2-\sigma\right)\eta_{j-2}+4\left(4+\sigma\right)\eta_{j-1}-6\left(6+\sigma\right)\eta_j+4\left(4+\sigma\right)\eta_{j+1}+\left(2-\sigma\right)\eta_{j+2}\right). \tag{10}$$

3. Description of Scheme

This section presents the scheme in both temporal and spatial directions[25].

Temporal Discretization

Consider the time interval $[0,T]$ by taking the knots $0=t_0<t_1<\ldots<t_z=T,$

Where $t_m=m\Delta t$ and $m=0,\ 1,2,\ \ldots,Z,$ subdivided into Z equal subintervals of size $\Delta t=\dfrac{T}{Z}.$

We discretize the time derivative of the Allen–Cahn Equation (1) at $t = t_{m+1}$ as:

$$\frac{\partial^{\gamma}}{\partial t^{\gamma}} q\left(p, t_{m+1}\right) = \frac{1}{\Gamma\left(1-\alpha\right)} \int_{0}^{t_{m+1}} \frac{\partial}{\partial \tau} q\left(p,\tau\right) \frac{1}{\left(t_{m+1}-\tau\right)\gamma} d\tau, \qquad 0 < \sigma < 1, \tag{11}$$

$$= \frac{1}{\Gamma\left(1-\alpha\right)} \sum_{s=0}^{m} \int_{0}^{t_{m+1}} \frac{\partial}{\partial \tau} q\left(p,\tau\right) \frac{1}{\left(t_{m+1}-\tau\right)\gamma} d\tau, \tag{12}$$

Using forward difference formulation, Equation (12) becomes

$$\frac{\partial^{\gamma}}{\partial t^{\gamma}} q\left(p, t_{m+1}\right) = \frac{1}{\Gamma\left(1-\alpha\right)} \sum_{s=0}^{m} \frac{q\left(p,t_{s+1}\right) - q\left(p,t_{s}\right)}{\Delta t} \int_{t_s}^{t_{s+1}} \frac{1}{\left(t_{m+1}-\tau\right)\gamma} d\tau + \sigma_{\Delta t}^{m+1}$$

$$= \frac{1}{\Gamma\left(1-\alpha\right)} \sum_{s=0}^{m} \frac{q\left(p,t_{s+1}\right) - q\left(p,t_{s}\right)}{\Delta t} \int_{t_{m-s}}^{t_{m-s+1}} \frac{1}{\left(\rho\right)^{\gamma}} d\rho + \sigma_{\Delta t}^{m+1}$$

$$= \frac{1}{\Gamma\left(1-\alpha\right)} \sum_{s=0}^{m} \frac{q\left(p,t_{m-s+1}\right) - q\left(p,t_{m-s}\right)}{\Delta t} \int_{t_s}^{t_{s+1}} \frac{1}{\left(\rho\right)^{\gamma}} d\rho + \sigma_{\Delta t}^{m+1}$$

$$= \frac{1}{\Gamma\left(2-\alpha\right)} \sum_{s=0}^{m} \frac{q\left(p,t_{m-s+1}\right) - q\left(p,t_{m-s}\right)}{\left(\Delta t\right)^{\gamma}} \left[\left(\ell+1\right)^{1-\gamma} - \left(\ell\right)^{1-\gamma}\right] + \sigma_{\Delta t}^{m+1}$$

$$\frac{\partial \gamma}{\partial t \gamma} q(p, t_{m+1}) = \frac{1}{\Gamma(2-\alpha)} \sum_{s=0}^{m} \xi^{\tau}{}_{s} \frac{q(p,t_{m-s+1}) - q(p,t_{m-s})}{(\Delta t)^{\gamma}} + \sigma_{\Delta t}^{m+1} \tag{13}$$

Where $\rho = t_{m+1} - \tau, \xi_s = \left(\ell+1\right)^{1-\alpha} - \left(\ell\right)^{1-\alpha}$ and the truncation error $\sigma_{\Delta t}^{m+1}$ is bounded as:

$$\left|\sigma_{\Delta t}^{m+1}\right| \le \delta \left(\Delta t\right)^{2-\gamma}, \tag{14}$$

Where δ is the finite constant

Lemma1. The coefficient ξ_s satisfy the following characteristics

- $\xi_s > 0$ and $\xi_s = 1$, $s = 1,\ 2,\ 3, \ldots,\ m.$
- $\xi_0 > \xi_1 > \xi_2 > \ldots > \xi_s, \xi_s \to 0$ as $s \to \infty$,

- $\sum_{s=0}^{m}(\xi_s-\xi_{s+1})+\xi_{m+1}=(1-\xi_1)+\sum_{s=1}^{m-1}(\xi_s-\xi_{s+1})+\xi_m=1$

Fully Implicit Scheme

Here, a fully implicit scheme is applied to discretize the time derivative. This scheme is linear that has an accuracy of second order in time[26].

Let $q_j^m=q(p_j,t^m),(q(p,t))^3=F(q(p,t))$ and substitute

$v(p,t_{m+1})-F(q(p,t))=\frac{1}{n}g^{m+1}.\eta_j^m=\eta_j(t^m)$ for $j=0,1,2,\ldots,n$ and $m=0,1,2,\ldots,Z.$

For $j=1,\ 2,\ldots,n-1,$ substitute Equation (6) and (10) in Equation (1), we have

$$\frac{1}{\Gamma(2-\gamma)(\Delta t)^{\gamma}}\ \sum_{s=0}^{m}\xi_s$$

$$\left[\frac{(4-\sigma)}{24}\eta_{j-1}^{m-s+1}+\frac{(8+\sigma)}{12}\eta_j^{m-s+1}+\frac{(4-\sigma)}{24}\eta_{j+1}^{m-s+1}-\frac{(4-\sigma)}{24}\eta_{j-1}^{m-s}-\frac{(8+\sigma)}{12}\eta_j^{m-s}-\frac{(4-\sigma)}{24}\eta_{j+1}^{m-s}\right]$$

$$-\frac{1}{24h^2}\ \left[(2-\sigma)\eta_{j-2}^{m+1}+4(4+\sigma)\eta_{j-1}^{m+1}-6(6+\sigma)\eta_j^{m+1}+4(4+\sigma)\eta_{j+1}^{m+1}+(2-\sigma)\eta_{j+2}^{m+1}\right]$$

$$-\left[\frac{(4-\sigma)}{24}\eta_{j-1}^{m+1}+\frac{(8+\sigma)}{12}\eta_j^{m+1}+\frac{(4-\sigma)}{24}\eta_{j+1}^{m+1}\right]=\delta^{m+1} \qquad (15)$$

Simplification of the above equation yields

$$[r\upsilon_1-l_8-\upsilon_1]\eta_{j-1}^{m+1}+[r\upsilon_2-l_9-\upsilon_2]\eta_j^{m+1}+[r\upsilon_1-l_8-\upsilon_1]\eta_{j-1}^{m+1}\ -l_7\eta_{j-2}^{m+1}-l_7\eta_{j+2}^{m+1}$$

$$= r\left[\upsilon_1\eta_{j-1}^m+\upsilon_2\eta_j^m+\upsilon_1\eta_{j+1}^m\right]$$

$$-r\sum_{s=1}^{m}\xi_s\left[\upsilon_1(\eta_{j-1}^{m-s+1}-\eta_{j-1}^{m-s})+\upsilon_2(\eta_j^{m-s+1}-\eta_j^{m-s})+\upsilon_1(\eta_{j+1}^{m-s+1}-\eta_{j+1}^{m-s})\right]+g^{m+1} \qquad (16)$$

For $j=0,$ substitute Equation (6) and (9) in Equation (1), we obtain

$$[r\upsilon_1-l_1-\upsilon_1]\eta_{-1}^{m+1}+[r\upsilon_2-l_2-\upsilon_2]\eta_0^{m+1}+[r\upsilon_1-l_3-\upsilon_1]\eta_1^{m+1}\ -l_4\eta_2^{m+1}\ -l_5\eta_3^{m+1}\ -l_6\eta_4^{m+1}$$

$$= r\left[\upsilon_1\eta_{-1}^{m}+\upsilon_2\eta_{0}^{m}+\upsilon_1\eta_{1}^{m}\right]$$

$$-r\sum_{s=1}^{m}\xi_s\left[\upsilon_1\left(\eta_{-1}^{m-s+1}-\eta_{-1}^{m-s}\right)+\upsilon_2\left(\eta_{0}^{m-s+1}-\eta_{0}^{m-s}\right)+\upsilon_1\left(\eta_{1}^{m-s+1}-\eta_{1}^{m-s}\right)\right]+g^{m+1} \quad (17)$$

For j=n substitute Equation (6) and (11) in Equation (1), we

$$\left[r\upsilon_1-l_3-\upsilon_1\right]\eta_{n-1}^{m+1}+\left[r\upsilon_2-l_2-\upsilon_2\right]\eta_{n}^{m+1}+\left[r\upsilon_1-l_1-\upsilon_1\right]\eta_{n+1}^{m+1}-l_6\eta_{n-4}^{m+1}-l_5\eta_{n-3}^{m+1}-l_4\eta_{n-2}^{m+1}$$

$$= r\left[\upsilon_1\eta_{n-1}^{m}+\upsilon_2\eta_{n}^{m}+\upsilon_1\eta_{n+1}^{m}\right]-r$$

$$\sum_{s=1}^{m}\xi_s\left[\upsilon_1\left(\eta_{n-1}^{m-s+1}-\eta_{n-1}^{m-s}\right)+\upsilon_2\left(\eta_{n}^{m-s+1}-\eta_{n}^{m-s}\right)+\upsilon_1\left(\eta_{n+1}^{m-s+1}-\eta_{n+1}^{m-s}\right)\right]+g^{m+1}, \quad (18)$$

Where $\upsilon_1=\frac{(4-\sigma)}{24}$, $\upsilon_2=\frac{(8+\sigma)}{12}$, $\upsilon_3=\frac{1}{2h}$, $l_1=\frac{2(14-\sigma)}{24h^2}$, $l_2=\frac{3(3\sigma-22)}{24h^2}$,

$l_3=\frac{8(7-2\sigma)}{24h^2}$, $l_4=\frac{14(\sigma-2)}{24h^2}$, $l_5=\frac{6(2-\sigma)}{24h^2}$, $l_6=\frac{(\sigma-2)}{24h^2}$, $l_7=\frac{(2-\sigma)}{24h^2}$, $l_8=\frac{4(4+\sigma)}{24h^2}$, and $l_9=\frac{6(6+\sigma)}{24h^2}$

The above system contains $n+1$ linear equation in $n+3$ unknowns. To obtain a unique solution, two more equations are obtained from the BCs [27]. Hence, a matrix system of dimension $(n+3)\times(n+3)$ is acquired

$$A\eta^{m+1}=B\left(\xi_m\eta^{0}+\sum_{s=0}^{m-1}(\xi_s-\xi_{s+1})\eta^{m-s}\right)+G, \quad (19)$$

$$\text{A}=\begin{bmatrix} v_1 & v_2 & v_3 & & & & & & & & \\ y_1 & y_2 & y_3 & & y_4 & & y_5 & & & & \\ & y_1 & y_2 & & y_3 & & y_4 & y_5 & & & \\ & & & \ddots & \ddots & \ddots & & & & & \\ & & & & & & y_1 & y_2 & y_3 & y_4 & y_5 \\ & & & & & & & y_1 & y_2 & y_3 & y_4 \\ & & & & & & & v_1 & v_2 & v_3 & \end{bmatrix}$$

$$B=\begin{bmatrix} 0 & 0 & 0 & & & & & & \\ v_1 & v_2 & v_1 & & & & & & \\ & v_1 & v_2 & v_1 & & & & & \\ & & \ddots & \ddots & \ddots & & & & \\ & & & & v_1 & v_2 & v_1 & & \\ & & & & & v_1 & v_2 & v_1 & \\ & & & & & 0 & 0 & 0 & \end{bmatrix}$$

$$\eta^m=\begin{bmatrix} \eta_{-1}^m \\ \eta_0^m \\ \eta_1^m \\ \vdots \\ \eta_{n-1}^m \\ \eta_n^m \\ \eta_{n+1}^m \end{bmatrix} \text{ and } \quad G=\begin{bmatrix} \psi_1^{m+1} \\ g_0^{m+1} \\ g_1^{m+1} \\ \vdots \\ g_{n-1}^{m+1} \\ g_n^{m+1} \\ \psi_2^{m+1} \end{bmatrix}$$

Where $y_1=rv_1-l_8-v_1$, $y_3=rv_1-l_8-v_1$ and $y_4=y_5=-l_7$.

In this section, a suitable initial vector $\eta^0=\left[\eta_{-1}^0,\eta_0^0,\cdots\eta_{n+1}^0\right]^T$ from IC is constructed to start iteration. The IC together with its derivatives is given as follows:

$$\left(q_p\right)_j^0=\frac{d}{dp}\left(\varphi\left(p_j\right)\right), \qquad j=0,\ n$$

And

$$q_j^0=q\left(p_j,0\right)=\sum_{j=1}^{n+1}\eta_j^0\left(0\right)C\left(p_j\right), \qquad j=0,1,\ldots,n.$$

The above system is a linear algebraic system of order $\left(n+3\right)\times\left(n+3\right),$ its matrix representation is given as:

$$D'\eta^0=H \qquad (20)$$

$$D' = \begin{bmatrix} v_3 & 0 & -v_3 & & & & & & \\ v_1 & v_2 & v_1 & & & & & & \\ & v_1 & v_2 & v_1 & & & & & \\ & & \ddots & \ddots & \ddots & & & & \\ & & & & v_1 & v_2 & v_1 & & \\ & & & & & v_1 & v_2 & v_1 & \\ & & & & & v_3 & 0 & -v_3 & \end{bmatrix} \text{ and } H = \begin{bmatrix} \varphi_0' \\ \varphi_0 \\ \varphi_1 \\ \vdots \\ \varphi_{n-1} \\ \varphi_n \\ \varphi_n' \end{bmatrix}$$

4. Stability Analysis:

In this section, we study the scheme's stability[29]. To check the stability of proposed technique we use Fourier series method. Suppose $Q\ (p,t)$ is the approximation of Equation (15). We define

$$\zeta_j^m = q_j^m - Q_j^m \qquad j = 1,\ldots,n-1, \quad m = 0,1,\ldots,Z \tag{21}$$

$$\zeta^m = \left[\zeta_1^m, \zeta_2^m, \ldots, \zeta_{n-1}^m\right]^T \tag{22}$$

Equation (21) satisfies Equation (15), the round- off error equation is given as:

$$\left[rv_1 - l_8 - v_1\right]\zeta_{j-1}^{m+1} + \left[rv_2 + l_9 - v_2\right]\zeta_j^{m+1} + \left[rv_1 - l_8 - v_1\right]\zeta_{j+1}^{m+1} - l_7\zeta_{j-2}^{m+1} - l_7\zeta_{j+2}^{m+1} = r\left[v_1\zeta_{j-1}^m + v_2\zeta_j^m + v_1\zeta_{j+1}^m\right]$$

$$-r\sum_{s=1}^{m}\xi_s\left[v_1\left(\zeta_{j-1}^{m-s+1} - \zeta_{j-1}^{m-s}\right) + v_2\left(\zeta_j^{m-s+1} - \zeta_j^{m-s}\right) + v_1\left(\zeta_{j+1}^{m-s+1} - \zeta_{j+1}^{m-s}\right)\right] \tag{23}$$

The IC and BCs become

$$\begin{cases} \zeta_j^0 = \varphi\left(p_j\right), j = 1,2,\ldots,n, \\ \zeta_0^m = \psi_1\left(t_m\right), \zeta_n^m = \psi_2\left(t_m\right), m = 0,1,\ldots,Z. \end{cases} \tag{24}$$

We define grid function as:

$$\zeta^m = \begin{cases} \zeta_j^m, p_j - \dfrac{h}{2} < p \le p_j + \dfrac{h}{2}, j = 1,2,\ldots,n-1 \\ 0, a \le p \le a + \dfrac{h}{2} orb - \dfrac{h}{2} \le p \le b. \end{cases} \tag{25}$$

The Fourier series representation of ζ^m is given as:

$$\zeta^m(p)=\sum_{n=-\infty}^{\infty}\sigma_m(n)e^{\left(\frac{2\pi inp}{b-a}\right)},\qquad m=1,2,\ldots,Z. \tag{26}$$

Were

$$\sigma^m(n)=\frac{1}{b-a}\int_a^b\zeta^m(p)e^{\left(\frac{-2\pi inp}{b-a}\right)}dp. \tag{27}$$

Definition of natural norm yields

$$\|\zeta\|_2=\left(\sum_{j=1}^{n-1}h\left|\zeta_j^m\right|^2\right)^{\frac{1}{2}}$$

$$=\left[\int_a^{a+\frac{h}{2}}\left|\zeta^m\right|^2dp+\sum_{j=1}^{Z-1}\int_{p_j-\frac{h}{2}}^{p_j+\frac{h}{2}}\left|\zeta^m\right|^2dp+\int_{b-\frac{h}{2}}^{b}\left|\zeta^m\right|^2dp\right]^{\frac{1}{2}}$$

$$=\left[\int_a^b\left|\zeta^m\right|^2dp\right]^{\frac{1}{2}}$$

Using the Perceval's identity, we have

$$\int_a^b\left|\zeta^m\right|^2dp=\sum_{-\infty}^{\infty}\left|\sigma_m(r)\right|^2$$

Thus, we obtain

$$\|\zeta\|_2^2=\sum_{-\infty}^{\infty}\left|\sigma_m(r)\right|^2 \tag{28}$$

Consider form as: the solution in Fourier series

$$\zeta_k^m=\sigma_m e^{i\theta kh}, \tag{29}$$

Where $i=(-1)^{\frac{1}{2}}$ and $\theta=\dfrac{2\pi m}{b-a}$. Substituting Equation (29) in (23), we achieve

$$\left[rv_1-l_8-v_1\right]\sigma_{m+1}e^{i\theta(k-1)h}+\left[rv_2-l_9-v_2\right]\sigma_{m+1}e^{i\theta kh}+\left[rv_1-l_8-v_1\right]\sigma_{m+1}e^{i\theta(k+1)h} \tag{30}$$

$$-l_7\sigma_{m+1}\left(e^{i\theta(k-2)h}+e^{i\theta(k+2)h}\right)=r\sigma_m\left[v_1e^{i\theta(k-1)h}+v_2e^{i\theta kh}+v_1e^{i\theta(k+1)h}\right]-r$$

$$\sum_{s=1}^{m}\xi_s\left[v_1\left(\sigma_{m-s+1}e^{i\theta(k-1)h}-\sigma_{m-s}e^{i\theta(k-1)h}\right)+v_2\left(\sigma_{m-s+1}e^{i\theta kh}-\sigma_{m-s}e^{i\theta kh}\right)+v_1\left(\sigma_{m-s+1}e^{i\theta(k+1)h}-\sigma_{m-s}e^{i\theta(k+1)h}\right)\right]$$

Simplification of the above equation yields

$$\sigma_{m+1}=\frac{1}{u_1}\sigma_m-\frac{1}{u_1}\sum_{s=1}^{m}\xi_s\left(\zeta_{m-s+1}-\zeta_{m-s}\right) \tag{31}$$

Were

$$u_1=1+\frac{-12+2\sin^2\left(\theta\frac{h}{2}\right)\left(4\left(4+\sigma\right)-\left(4\left(-\sigma\right)h^2\right)+2\sin^2\left(\theta h\right)\left(2-\sigma\right)\right)}{12h^2r\left(1+\frac{\sigma-4}{6}\right)\sin^2\left(\theta\frac{h}{2}\right)} \tag{32}$$

$$u_1\geq 1 \text{ for } \sigma>-2$$

It is clear that

Proposition 1. Assume that σ_m, $m=1,\ 2,\ldots,T\times Z,$ satisfy Equation (31), we have

$$\left|\sigma_m\right|\leq\left|\sigma_0\right| \tag{33}$$

Proof: To verify inequality (33), we use mathematical induction. Put m=0 in (31), we obtain

$$\left|\sigma_{m+1}\right|\leq\frac{1}{u_1}\left|\sigma_n\right|-\frac{1}{u_1}\sum_{s=1}^{m}\left(\sigma_{m-s+1}-\sigma_{m-s}\right)$$

Assume that $\left|\sigma_m\right|\leq\left|\sigma_0\right|$ is true for $m=1,2,\ldots,T\times Z\ -1.$ From Equation (31), we obtain

$$\left|\sigma_{m+1}\right|\leq\frac{1}{u_1}\left|\sigma_n\right|-\frac{1}{u_1}\sum_{s=1}^{m}\left(\sigma_{m-s+1}-\sigma_{m-s}\right)$$

$$\leq\frac{1}{u_1}\left|\sigma_0\right|-\frac{1}{u_1}\sum_{s=1}^{m}\left(\sigma_0-\sigma_0\right)$$

Hence, inequality (33) is true.

Theorem 1. The scheme (15) is unconditionally stable.

Proof: Using above proposition and Equation (28), we acquire

$$\left\|\zeta^{m}\right\|_{2} \leq \left\|\zeta^{0}\right\|_{2}, \qquad m=1,2,\ldots,\ Z,$$

Hence, Equation (15) with IC and BCs is unconditionally stable.

5. Convergence:

In this section, convergence of the proposed method is examined that is based on Adalberto and Aurora's technique

Theorem 2. Suppose that

$q(p,t) \in C^{4}[a,b], v \in C^{2}[a,b]$ $\Theta = [a = p_0, p_1, ..., p_n = b]$ is the equidistant partition of $[a,b]$ having length h. Consider $Q(p,t)$ is a unique spline that interpolates the solution of the propounded problem at knots $p_0, p_1, ..., p_n \in \Theta$, then there exists a constant C_j that does not dependent on h, so $\forall t \geq 0$,we have

$$\left\|D^{j}\left(q(p,t)-Q(p,t)\right)\right\|_{\infty} \leq c_j h^{4-j},\ j=0,\ 1,\ 2. \tag{34}$$

Lemma 2 The Hybrid CBS set $\{C_{-1}, C_0, ..., C_{n+1}\}$ defined in (4) satisfies the following inequality

$$\sum_{j=-1}^{n+1} \left|C_j(p,\sigma)\right| \leq \frac{7}{4} \qquad 0 \leq p \leq 1 \tag{35}$$

Theorem 3. Consider the approximation for the exact solution $q(p,t)$ is $Q(p,t)$ of the time dependent FPDEs. Further, if $v \in C^{2}[0,1]$, then the inequality

$$\left\|q(p,t)-Q(p,t)\right\|_{\infty} \leq \Phi h^{2} \tag{36}$$

Exists for every $t \geq 0$, h is sufficiently small and Φ is a positive constant not depending on h.

Proof: Consider the calculated spline approximation is $Q(p,t)$ to the approximate solution $Q(p,t)$ where $\tilde{Q}(p,t) = \sum_{j=-1}^{n+1} \breve{d}_j C_k(p)$. From triangular inequality, we obtain

$$\left\|q(p,t)-Q(p,t)\right\|_{\infty} \leq \left\|q(p,t)-\tilde{Q}(p,t)\right\|_{\infty} + \left\|\tilde{Q}(p,t)-Q(p,t)\right\|_{\infty} \tag{37}$$

From inequality (34), we have

$$\left\| D^j \left(q(p,t) - \tilde{Q}(p,t) \right) \right\|_\infty \le c_j h^{4-j}, j = 0,1,2. \tag{38}$$

Using Equation (37), we achieve

$$\left\| \left(q(p,t) - Q(p,t) \right) \right\|_\infty \le c_0 h^4 + \left\| \left(\tilde{Q}(p,t) - Q(p,t) \right) \right\|_\infty \tag{39}$$

The collocation conditions are:

Let

$$L\tilde{Q}(p,t) = \bar{g}(p_j,t), j = 0,1,\ldots,n.$$

Therefore, the difference equation $L\left(\tilde{Q}(p_j,t) - Q(p_j,t)\right)$ of the given problem for any time level m is describe as

$$\left[rv_1 - l_8 - v_1\right]\varsigma_{j-1}^{m+1} + \left[rv_2 + l_9 - v_2\right]\varsigma_j^{m+1} + \left[rv_1 - l_8 - v_1\right]\varsigma_{j+1}^{m+1} - l_7\varsigma_{j-2}^{m+1} - l_7\varsigma_{j+2}^{m+1}$$

$$= r\left[v_1\varsigma_{j-1}^m + v_2\varsigma_j^m + v_1\varsigma_{j+1}^m\right]$$

$$-r\sum_{s=1}^{m}\xi_s\left[v_1\left(\varsigma_{j-1}^{m-s+1} - \varsigma_{j-1}^{m-s}\right) + v_2\left(\varsigma_j^{m-s+1} - \varsigma_j^{m-s}\right) + v_1\left(\varsigma_{j+1}^{m-s+1} - \varsigma_{j+1}^{m-s}\right)\right] + g^{m+1}, \tag{40}$$

For $j = 0, n,$ we have

$$\left[rv_1 - l_1 - v_1\right]\varsigma_{-1}^{m+1} + \left[rv_2 + l_2 - v_2\right]\varsigma_0^{m+1} + \left[rv_1 - l_3 - v_1\right]\varsigma_1^{m+1} - l_4\varsigma_2^{m+1} - l_5\varsigma_3^{m+1} - l_6\varsigma_4^{m+1}$$

$$= r\left[v_1\varsigma_{-1}^m + v_2\varsigma_0^m + v_1\varsigma_1^m\right]$$

$$-r\sum_{s=1}^{m}\xi_s\left[v_1\left(\varsigma_{-1}^{m-s+1} - \varsigma_{-1}^{m-s}\right) + v_2\left(\varsigma_0^{m-s+1} - \varsigma_0^{m-s}\right) + v_1\left(\varsigma_1^{m-s+1} - \varsigma_1^{m-s}\right)\right] + g^{m+1}, \tag{41}$$

And

$$\left[rv_1 - l_3 - v_1\right]\varsigma_{n-1}^{m+1} + \left[rv_2 + l_2 - v_2\right]\varsigma_n^{m+1} + \left[rv_1 - l_1 - v_1\right]\varsigma_{n+1}^{m+1} - l_6\varsigma_{n-4}^{m+1} - l_5\varsigma_{n-3}^{m+1} - l_4\varsigma_{n-2}^{m+1} =$$

$$r\left[v_1\varsigma_{n-1}^m + v_2\varsigma_n^m + v_1\varsigma_{n+1}^m\right] - r\sum_{s=1}^{m}\xi_s\left[v_1\left(\varsigma_{n-1}^{m-s+1} - \varsigma_{n-1}^{m-s}\right) + v_2\left(\varsigma_n^{m-s+1} - \varsigma_n^{m-s}\right) + v_1\left(\varsigma_{n+1}^{m-s+1} - \varsigma_{n+1}^{m-s}\right)\right] + g^{m+1}$$

The BCs for Equation (41) and (42) are

$$v_1\varsigma_{-1}^{m+1}+v_2\varsigma_0^{m+1}+v_1\varsigma_1^{m+1}=0,$$

$$.\,v_1\varsigma_{n-1}^{m+1}+v_2\varsigma_n^{m+1}+v_1\varsigma_{n+1}^{m+1}=0,$$

Were

$$\varsigma_j^m=\eta_j^m-\breve{d}_j^m \qquad j=-1,0,1,\ldots,n+1.$$

Using (3.38), we obtain

$$K_j^m=h^2\left[g_j^m-\bar{g}_j^m\right]\le ch^4 \qquad j=0,1,2,\ldots,n.$$

Define

$K_j^m=\max\left\{\left|K_j^m\right|;0\le j\le n\right\},\breve{e}_j^m=\left|\varsigma_j^m\right|$ And $\breve{e}^m=\max\left\{\left|\breve{e}_j^m\right|;0\le j\le n\right\},$

Put m=0 in Equation (40), we obtain

$$\left[rv_1-l_8-v_1\right]\varsigma_{j-1}^1+\left[rv_2+l_9-v_2\right]\varsigma_j^1+\left[rv_1-l_8-v_1\right]\varsigma_{j+1}^1-l_7\varsigma_{j-2}^1-l_7\varsigma_{j+2}^1$$

$$=r\left[v_1\varsigma_{j-1}^0+v_2\varsigma_j^0+v_1\varsigma_{j+1}^0\right]+g^1$$

Using IC, $\breve{e}^0=0$

$$\left[rv_2+l_9-v_2\right]\varsigma_j^1=-\left[rv_1-l_8-v_1\right]\left[\varsigma_{j-1}^1+\varsigma_{j+1}^1\right]+l_7\left[\varsigma_{j-2}^1+\varsigma_{j+2}^1\right]+\frac{1}{h^2}K_j^1$$

Taking absolute values of ς_j^m and K_j^m ,we achieve

$$\breve{e}_j^1\le\frac{6ch^4}{h^2r(2+\sigma)+4\sigma-h^2(2+\sigma)+16}$$

Put $m=0$,in Equation (3.41) and (3.42), we acquire

$$\left[rv_1-l_1-v_1\right]\varsigma_{-1}^1+\left[rv_2+l_2-v_2\right]\varsigma_0^1+\left[rv_1-l_3-v_1\right]\varsigma_1^1-l_4\varsigma_2^1-l_5\varsigma_3^1-l_6\varsigma_4^1$$

$$=r\left[v_1\varsigma_{-1}^0+v_2\varsigma_0^0+v_1\varsigma_1^0\right]+g^1,$$

And

$$\left[rv_1 - l_3 - v_1\right]\varsigma_{n-1}^1 + \left[rv_2 + l_2 - v_2\right]\varsigma_n^1 + \left[rv_1 - l_1 - v_1\right]\varsigma_{n+1}^1 - l_6\varsigma_{n-4}^1 - l_5\varsigma_{n-3}^1 - l_4\varsigma_{n-2}^1$$

$$= r\left[v_1\varsigma_{n-1}^0 + v_2\varsigma_n^0 + v_1\varsigma_{n+1}^0\right] + g^1,$$

Using IC, $\breve{e}^0 = 0$:

$$\left[rv_2 + l_2 - v_2\right]\varsigma_0^1 = -\left[rv_1 - l_1 - v_1\right]\varsigma_{-1}^1 - \left[rv_1 - l_3 - v_1\right]\varsigma_{+1}^1 + l_4\varsigma_2^1 + l_5\varsigma_3^1 + l_6\varsigma_4^1 + \frac{1}{h^2}K_0^1$$

And

$$\left[rv_2 + l_2 - v_2\right]\varsigma_n^1 = -\left[rv_1 - l_3 - v_1\right]\varsigma_{n-1}^1 - \left[rv_1 - l_1 - v_1\right]\varsigma_{n+1}^1 + l_6\varsigma_{n-4}^1 + l_5\varsigma_{n-3}^1 + l_4\varsigma_{n-2}^1 + \frac{1}{h^2}K_n^1 \quad (42)$$

Taking absolute values of ς_0^1 and K_0^1,we have

$$\breve{e}_0^1 \le \frac{6ch^4}{h^2 r(2+\sigma) - 9\sigma - h^2(2+\sigma) + 42}$$

Also, for $j = n$

$$\breve{e}_n^1 \le \frac{6ch^4}{h^2 r(2+\sigma) - 9\sigma - h^2(2+\sigma) + 42}$$

Using BCs, we conclude that

$$\breve{e}_{-1}^1 \le c_1 h^2, \breve{e}_{n+1}^1 \le c_1 h^2 \quad (43)$$

Hence

$$\breve{e}^1 \le c_1 h^2 \quad (44)$$

Where c_1 is independent of h.

Using induction procedure on m, suppose that $\breve{e}_j^y \le c_y h^2$ for $y = 1, 2, \ldots, m.$

Let $c = \max\left\{c_y : 0 \le y \le m\right\}$ .Then, the Equation (40) becomes

$$\left[rv_1 - l_8 - v_1\right]\varsigma_{j-1}^{m+1} + \left[rv_2 + l_9 - v_2\right]\varsigma_j^{m+1} + \left[rv_1 - l_8 - v_1\right]\varsigma_{j+1}^{m+1} - l_7\varsigma_{j-2}^{m+1} - l_7\varsigma_{j+2}^{m+1}$$

$$= r\xi_0\left[v_1\varsigma_{j-1}^m + v_2\varsigma_j^m + v_1\varsigma_{j+1}^m\right] - r[\xi_1\left(v_1\left(\varsigma_{j-1}^m - \varsigma_{j-1}^{m-1}\right) + v_2\left(\varsigma_j^m - \varsigma_j^{m-1}\right) + v_1\left(\varsigma_{j+1}^m - \varsigma_{j+1}^{m-1}\right)\right)$$

$$\xi_2\left(v_1\left(\varsigma_{j-1}^{m-1} - \varsigma_{j-1}^{m-2}\right) + v_2\left(\varsigma_j^{m-1} - \varsigma_j^{m-2}\right) + v_1\left(\varsigma_{j+1}^{m-1} - \varsigma_{j+1}^{m-2}\right)\right) + \ldots +$$

$$\xi_m\left(v_1\left(\varsigma_{j-1}^1 - \varsigma_{j-1}^0\right) + v_2\left(\varsigma_j^1 - \varsigma_j^0\right) + v_1\left(\varsigma_{j+1}^1 - \varsigma_{j+1}^0\right)\right) \ ] + g^{m+1},$$

Taking absolute value of ς_j^m and K_j^m ,we obtain

$$\breve{e}_j^{m+1} \le \frac{6ch^4}{h^2 r(2+\sigma) + 4\sigma - h^2(2+\sigma) + 16}\left(r\sum_{s=0}^{m}(\xi_s - \xi_{s+1})ch^2 + ch^2\right)$$

Also from BCs:

$$\breve{e}_j^{m+1} \le ch^2$$

Thus, $\forall m$,we have

$$\breve{e}_j^{m+1} \le ch^2 \tag{45}$$

From above equation and Lemma 2, we have.

$$\tilde{Q}(p,t) - Q(p,t) = \sum_{j=-1}^{n+1}\left(\breve{d}_j(t) - \eta_j(t)\right)C_j(p,\sigma)$$

Taking the norm, we obtain

$$\left\|q(p,t) - \tilde{Q}(p,t)\right\|_\infty \le 1.75ch^2$$

Using above inequality and Equation (45), we achieve

$$\left\|q(p,t) - \tilde{Q}(p,t)\right\|_\infty + \left\|\tilde{Q}(p,t) - Q(p,t)\right\|_\infty \le c_0h^4 + 1.75ch^2 = \Phi h^2,$$

Where $\Phi = c_0h^2 + 1.75c$

Equation (14) and previous theorem show that the proposed method converges, i.e.

$$\left\|q(p,t) - \tilde{Q}(p,t)\right\|_\infty \le \Phi h^2 + \delta(\Delta t)^{2-\gamma},$$

Where Φ and δ are constants.

7. Numerical Results

Two numerical examples are demonstrated for ACE to examine the efficiency of proposed scheme [30]. To test the scheme, the error norms L_2, L_∞ and relative error are used. These are defined as:

$$L_2 = \sqrt{h\sum_{j=0}^{n}\left|Q\left(p_j,t\right)-q\left(p_j,t\right)\right|^2}, L_\infty = \max_{0\le j\le n}\left|Q\left(p_j,t\right)-q\left(p_j,t\right)\right|$$

$$\text{Relative error} = \left|\frac{Q\left(p_j,t\right)-q\left(p_j,t\right)}{q\left(p_j,t\right)}\right|$$

All the calculations are performed with the help of Mathematica 9.0 software.

Problem 1.

Consider the Allen–Cahn equation

$$\frac{\partial^\alpha q}{\partial t^\alpha}-\frac{\partial^2 q}{\partial p^2}+q^3-q(p,t)=v(p,t) \quad \mathrm{p}\in[\mathrm{a},\mathrm{b}],\quad \mathrm{t}\in[0,\mathrm{T}],$$

The source term $v(p,t)$ is given as $v(p,t)=(\alpha+1)(p-1)pt\Gamma(1+\alpha)+(\mathrm{p}^2-\mathrm{p})^{3t^3+3\alpha}-(p^2-p+2)\,\mathrm{t}^{1+\alpha}$

$v(p,t)=(\alpha+1)(p-1)pt\Gamma(1+\alpha)+(\mathrm{p}^2-\mathrm{p})^{3t^3+3\alpha}-(p^2-p+2)\,\mathrm{t}^{1+\alpha}$

$v(p,t)=p(p^2-1)^3\,pt^{2-\alpha}E_{1,3-\alpha}(t)+6(7p^4-10p^2+3)pt^2E_{1,3}(t)+\frac{1}{2}q(p,t)[\mathrm{q}$

$$\mathrm{E}_{\varepsilon,\mathrm{v}}=\sum_{k=0}^{\infty}\frac{\omega^k}{\Gamma(\varepsilon k+\alpha)}.$$

Initial condition	$u(x,0)=0$	$0\le x\le 1$
Boundary condition	$u(0,t)=0,\quad u(1,t)=0,$	$t\ge 0$

. The maximum absolute error is demonstrated in Tables 1 and 2 for different values of p by taking $\alpha=\frac{7}{10},\frac{9}{10}$, $n=100,\ p\in[0,1],\Delta t=\frac{1}{100}$

And $t=1$. In Table 3, L_2 and L_∞ norms are expounded for $\alpha=\frac{2}{10},\ \frac{5}{10},\ \frac{8}{10}$ different values of t. Figure 1 represent the physical behavior of exact and approximate results against various values of time for $\alpha=\frac{4}{10}$, $n=60,\Delta t=\frac{1}{1000}$ and

$p \in [-1, 2]$. The 3D graphical representation for exact and numerical solutions when $n = 80, t = \frac{2}{10}$, $\gamma = \frac{6}{10}$ and $\Delta t = \frac{1}{1000}$ is shown in Figure 2. True and numerical solutions for distinct values of γ are exhibited in Figure 3. A comparison of three-dimensional graphs for $n = 100, t = \frac{2}{10}$, $\alpha = \frac{4}{10}$ and $\Delta t = \frac{1}{100}$ is presented in Figure 4.

Table 1. Absolute error at $t = 1$ whereas $\alpha = \frac{7}{10}$, $\Delta t = \frac{1}{1000}$ and $n = 100$ for Problem 1 using proposed Scheme.

p/t →	$\frac{1}{10}$	$\frac{2}{10}$	$\frac{3}{10}$	$\frac{4}{10}$	$\frac{5}{10}$	$\frac{6}{10}$	$\frac{7}{10}$	$\frac{8}{10}$	$\frac{9}{10}$
$\frac{1}{10}$	7.4669×10^{-7}	6.2604×10^{-7}	6.1886×10^{-7}	6.1350×10^{-7}	6.0561×10^{-7}	6.5886×10^{-7}	8.0346×10^{-7}	1.1454×10^{-6}	1.2058×10^{-6}
$\frac{2}{10}$	1.2691×10^{-6}	1.1984×10^{-6}	1.0911×10^{-6}	1.0453×10^{-6}	1.0731×10^{-6}	1.1017×10^{-6}	1.3715×10^{-6}	2.1338×10^{-6}	2.4504×10^{-6}
$\frac{3}{10}$	2.1109×10^{-6}	1.3783×10^{-6}	1.2327×10^{-6}	1.1735×10^{-6}	1.3189×10^{-6}	1.3089×10^{-6}	2.1017×10^{-6}	2.4714×10^{-6}	3.3063×10^{-6}
$\frac{4}{10}$	2.2548×10^{-6}	2.1833×10^{-6}	1.3139×10^{-6}	1.1477×10^{-6}	1.3075×10^{-6}	2.0424×10^{-6}	2.3234×10^{-6}	3.2402×10^{-6}	4.3002×10^{-6}
$\frac{5}{10}$	2.3726×10^{-6}	2.1878×10^{-6}	2.0105×10^{-6}	1.1421×10^{-6}	2.2074×10^{-6}	2.3589×10^{-6}	2.2720×10^{-6}	3.1424×10^{-6}	4.1841×10^{-6}
$\frac{6}{10}$	2.0548×10^{-6}	2.1833×10^{-6}	1.2139×10^{-6}	1.4477×10^{-6}	1.2075×10^{-6}	2.0424×10^{-6}	2.134×10^{-6}	3.2402×10^{-6}	4.3002×10^{-6}
$\frac{7}{10}$	2.1109×10^{-6}	1.1783×10^{-6}	1.3327×10^{-6}	1.2735×10^{-6}	1.3189×10^{-6}	1.2089×10^{-6}	2.1017×10^{-6}	2.3714×10^{-6}	3.1063×10^{-6}
$\frac{8}{10}$	1.2691×10^{-6}	1.1984×10^{-6}	1.0911×10^{-6}	1.0453×10^{-6}	1.0731×10^{-6}	1.2017×10^{-6}	1.4715×10^{-6}	2.1338×10^{-6}	2.3504×10^{-6}
$\frac{9}{10}$	7.3669×10^{-7}	6.2604×10^{-7}	6.1886×10^{-7}	6.1350×10^{-7}	6.0561×10^{-7}	6.1886×10^{-7}	8.2346×10^{-7}	1.1454×10^{-6}	1.2058×10^{-6}

Table 2. Absolute error at $t = 1$ whereas $\alpha = \frac{9}{10}, \Delta t = \frac{1}{1000}$ and $n = 100$ for problem 1 using proposed technique.

p/t →	$\frac{1}{10}$	$\frac{2}{10}$	$\frac{3}{10}$	$\frac{4}{10}$	$\frac{5}{10}$	$\frac{6}{10}$	$\frac{7}{10}$	$\frac{8}{10}$	$\frac{9}{10}$
$\frac{1}{10}$	3.4507×10^{-6}	3.4748×10^{-6}	3.3734×10^{-6}	3.4690×10^{-6}	3.2545×10^{-6}	3.4715×10^{-6}	3.3543×10^{-6}	3.6420×10^{-6}	4.6838×10^{-6}

$\frac{2}{10}$	5.4631×10^{-6}	6.6627×10^{-6}	6.1522×10^{-6}	6.7461×10^{-6}	6.4223×10^{-6}	6.2623×10^{-6}	7.5331×10^{-6}	7.6125×10^{-6}	8.2981×10^{-6}
$\frac{3}{10}$	7.5782×10^{-6}	9.4577×10^{-6}	9.2210×10^{-6}	9.7159×10^{-6}	9.3894×10^{-6}	9.1559×10^{-6}	9.4119×10^{-6}	1.6369×10^{-5}	1.6368×10^{-5}
$\frac{4}{10}$	9.6171×10^{-6}	1.1841×10^{-6}	1.0153×10^{-5}	1.0150×10^{-5}	1.0124×10^{-5}	1.0213×10^{-5}	1.2532×10^{-5}	1.1218×10^{-5}	1.2442×10^{-5}
$\frac{5}{10}$	9.3748×10^{-6}	1.0384×10^{-6}	1.0713×10^{-5}	1.3710×10^{-5}	1.0685×10^{-5}	1.0782×10^{-5}	1.4125×10^{-5}	1.1859×10^{-5}	1.2164×10^{-5}
$\frac{6}{10}$	9.1171×10^{-6}	1.1841×10^{-6}	1.0153×10^{-5}	1.0150×10^{-5}	1.024×10^{-5}	1.0213×10^{-5}	1.0532×10^{-5}	1.1218×10^{-5}	1.2442×10^{-5}
$\frac{7}{10}$	7.4782×10^{-6}	9.1577×10^{-6}	9.3210×10^{-6}	9.1159×10^{-6}	9.2894×10^{-6}	9.1559×10^{-6}	9.2119×10^{-6}	1.1369×10^{-5}	1.0368×10^{-5}
$\frac{8}{10}$	5.2631×10^{-6}	6.4627×10^{-6}	6.1522×10^{-6}	6.4461×10^{-6}	6.1223×10^{-6}	6.4623×10^{-6}	7.0331×10^{-6}	7.2125×10^{-6}	8.2981×10^{-6}
$\frac{9}{10}$	3.1507×10^{-6}	3.2748×10^{-6}	3.1734×10^{-6}	3.2690×10^{-6}	3.5545×10^{-6}	3.2715×10^{-6}	3.1543×10^{-6}	3.5420×10^{-6}	4.2838×10^{-6}

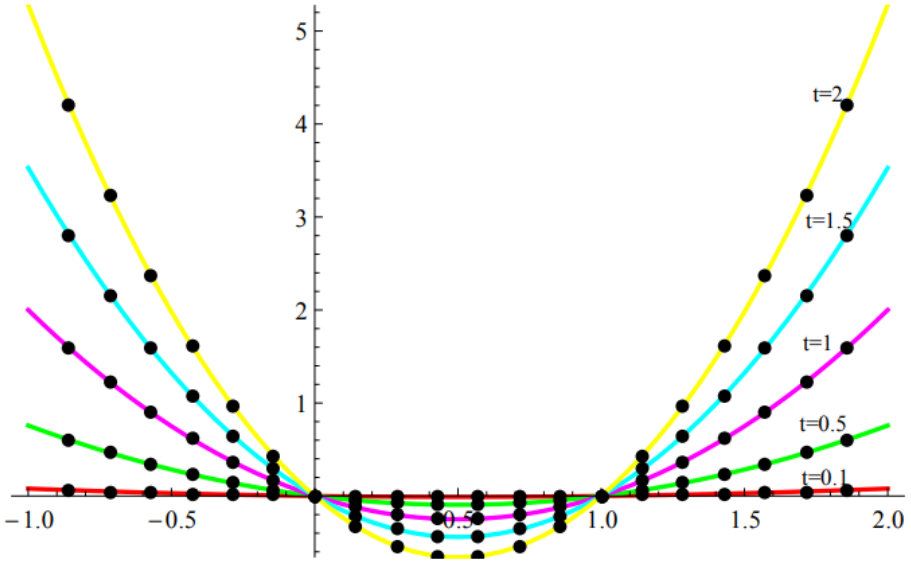

Figure 1. Comparison of exact and numerical solutions for Problem 1, when n = 60, $\Delta t = \frac{1}{1000}$, $\alpha = \frac{4}{10}$ and p ∈ [−1, 2].

Table 3. Error norms at $n = 64$ and $\Delta t = \frac{1}{1000}$ for Problem 1

T	$\alpha = \frac{2}{10}$		$\alpha = \frac{5}{10}$		$\alpha = \frac{8}{10}$	
	L_2	L_∞	L_2	L_∞	L_2	L_∞
$\frac{2}{10}$	5.5732×10^{-8}	7.5949×10^{-8}	2.4749×10^{-7}	3.3346×10^{-7}	3.5244×10^{-6}	2.3065×10^{-6}
$\frac{4}{10}$	2.3559×10^{-7}	4.3604×10^{-7}	3.4042×10^{-7}	4.6471×10^{-7}	3.7835×10^{-6}	4.5715×10^{-6}
$\frac{6}{10}$	8.5687×10^{-7}	1.7901×10^{-6}	7.6269×10^{-7}	1.5486×10^{-6}	3.7561×10^{-6}	4.4922×10^{-6}
$\frac{8}{10}$	1.4279×10^{-6}	2.2170×10^{-6}	1.6500×10^{-6}	2.2487×10^{-6}	4.6860×10^{-6}	6.8185×10^{-6}
1.0	3.5838×10^{-6}	4.6917×10^{-6}	3.2141×10^{-6}	5.1136×10^{-6}	6.3905×10^{-6}	9.7974×10^{-6}

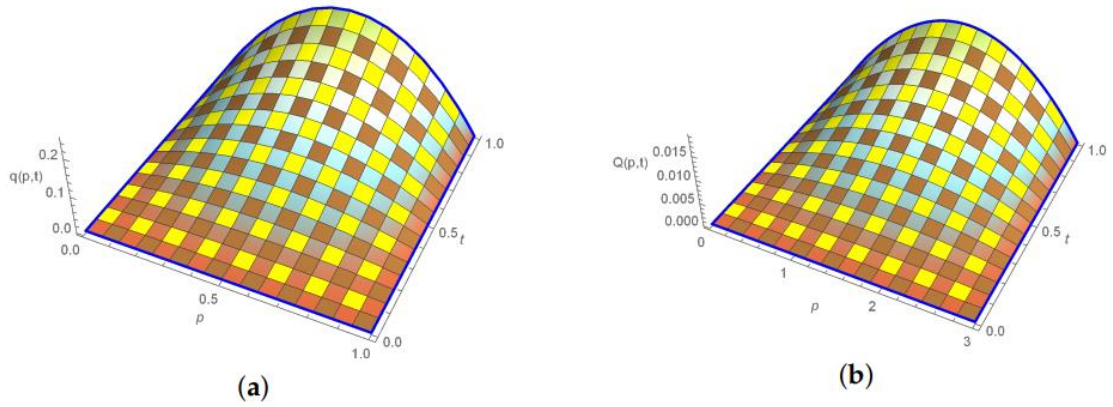

Figure 2. Three-dimensional graphs for n = 80, $\alpha = 6/10$, t = 2/10 and $\Delta t = \frac{1}{1000}$ of Problem 1.

(a) Exact solution. (b) Numerical solution

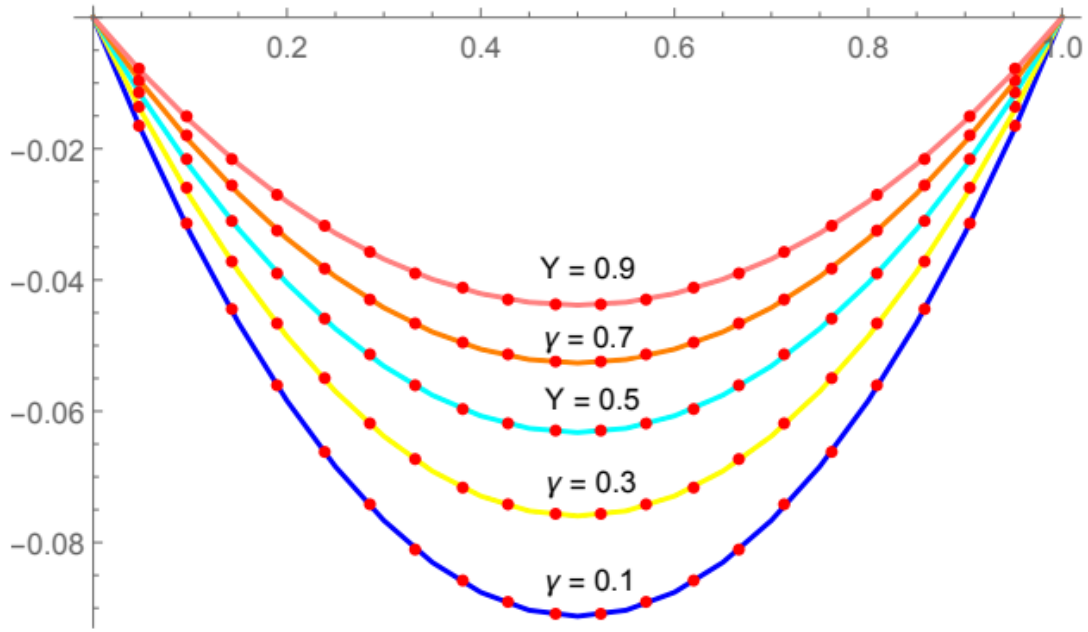

Figure 3. True and approximate solutions for Problem 1, when n = 20, t = 4/10 and p ∈ [0, 1] for different values of γ.

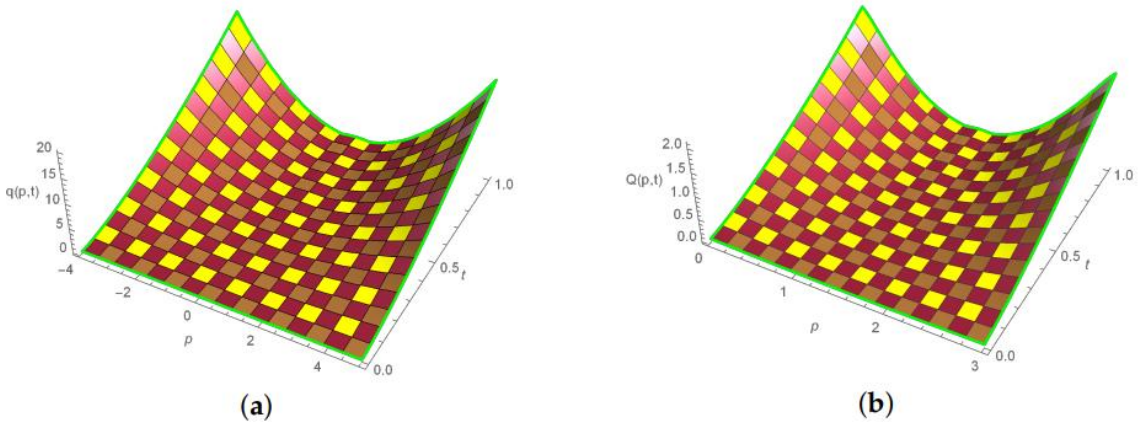

Figure 4. 3D graphs for Problem 1, when n = 100, $\alpha = 4/10$, t = 2/10 and p ∈ [−4, 5]. (a) Exact solution. (b) Numerical solution

Problem 2.

To demonstrate the efficiency and accuracy of the proposed numerical method, we consider the one-dimensional time fractional Allen–Cahn equation given by

$$\frac{\partial^{\alpha} u}{\partial t^{\alpha}} - \frac{\partial^{2} u}{\partial x^{2}} + u^{3} - u = v(p,t), \quad a \le p \le b, \quad 0 \le t \le T$$

The source term is given by $v(p,t) = p(p^2-1)^3 pt^{2-\alpha} E_{1,3-\alpha}(t) + 6(7p^4 - 10p^2 + 3)pt^2 E_{1,3}(t) + \frac{1}{2} q(p,t)[\mathrm{q(p,t)} - 1]$,

Where $\mathrm{E}_{\varepsilon,\mathrm{v}}(\omega)$ is the Mittag-Leffler function and is given $\mathrm{E}_{\varepsilon,\mathrm{v}} = \sum_{k=0}^{\infty} \frac{\omega^k}{\Gamma(\varepsilon k + \alpha)}$.

Table 4 represents contrast of the absolute error of proposed scheme with RCBS [31] for $\gamma = \frac{5}{10}, n = 10, t = \frac{1}{10}$ and $p \in [0,1]$. L_2 Norm is demonstrated in Table 5 for distinct values of α and t for $n = 16$ and $p \in [-1,1]$. The exact and computational solution are presented graphically in Figure 5 for $n = 100$, $\Delta t = \frac{1}{1000}$, $\alpha = \frac{6}{10}$ and $p \in [-1,1]$. Three-dimensional plot of exact and numerical solutions is shown in Figure 6.

Table 4. Absolute error at $t = \frac{1}{10}$ with $\alpha = \frac{5}{10}$, $n = 10$, $\Delta t = \frac{1}{1000}$ and $p \in [0,1]$ for Problem 2.

	Approximate Solution			*Error*		
ρ	*Exact Solution*	*RCBS* [31]	*Proposed Method*	*RCBS* [31]	*Proposed Method*	*Relative Error*
$\frac{1}{10}$	0.0005017	0.0005368	0.0005205	3.411×10^{-5}	2.584×10^{-5}	0.0574846
$\frac{2}{10}$	0.0009149	0.0009807	0.0009686	6.475×10^{-5}	5.264×10^{-5}	0.0586294
$\frac{3}{10}$	0.0011690	0.0012574	0.0012401	8.438×10^{-5}	7.519×10^{-5}	0.0608982
$\frac{4}{10}$	0.0012259	0.0013269	0.0012054	1.410×10^{-4}	7.349×10^{-5}	0.0648422
$\frac{5}{10}$	0.0010907	0.0011941	0.0011691	1.334×10^{-4}	7.738×10^{-5}	0.0718621
$\frac{6}{10}$	0.0008133	0.0009103	0.0008824	9.300×10^{-5}	6.416×10^{-5}	0.0850363
$\frac{7}{10}$	0.0004801	0.0005638	0.0005344	8.164×10^{-5}	5.329×10^{-5}	0.1130806
$\frac{8}{10}$	0.0001930	0.0002574	0.0002295	6.348×10^{-5}	3.457×10^{-5}	0.1894818
$\frac{9}{10}$	0.0000319	0.0000702	0.0000501	3.527×10^{-5}	1.319×10^{-5}	0.5702194

Table 5. L_2 norm for Problem 2 whereas $n=16$, $\Delta t=\frac{1}{100}$ and $p\in[-1,1]$.

t	$\alpha=\frac{2}{10}$	$\alpha=\frac{4}{10}$	$\alpha=\frac{6}{10}$	$\alpha=\frac{8}{10}$
$\frac{2}{10}$	4.0131×10^{-4}	3.4615×10^{-4}	3.3429×10^{-4}	3.2779×10^{-4}
$\frac{4}{10}$	1.5453×10^{-3}	1.5443×10^{-3}	1.4251×10^{-3}	1.3002×10^{-3}
$\frac{6}{10}$	4.4702×10^{-3}	4.5721×10^{-3}	4.5522×10^{-3}	3.6264×10^{-3}
$\frac{8}{10}$	9.6039×10^{-3}	8.5084×10^{-3}	8.6023×10^{-3}	8.6129×10^{-3}
1.0	1.5218×10^{-2}	1.0323×10^{-2}	1.3449×10^{-2}	1.6654×10^{-2}

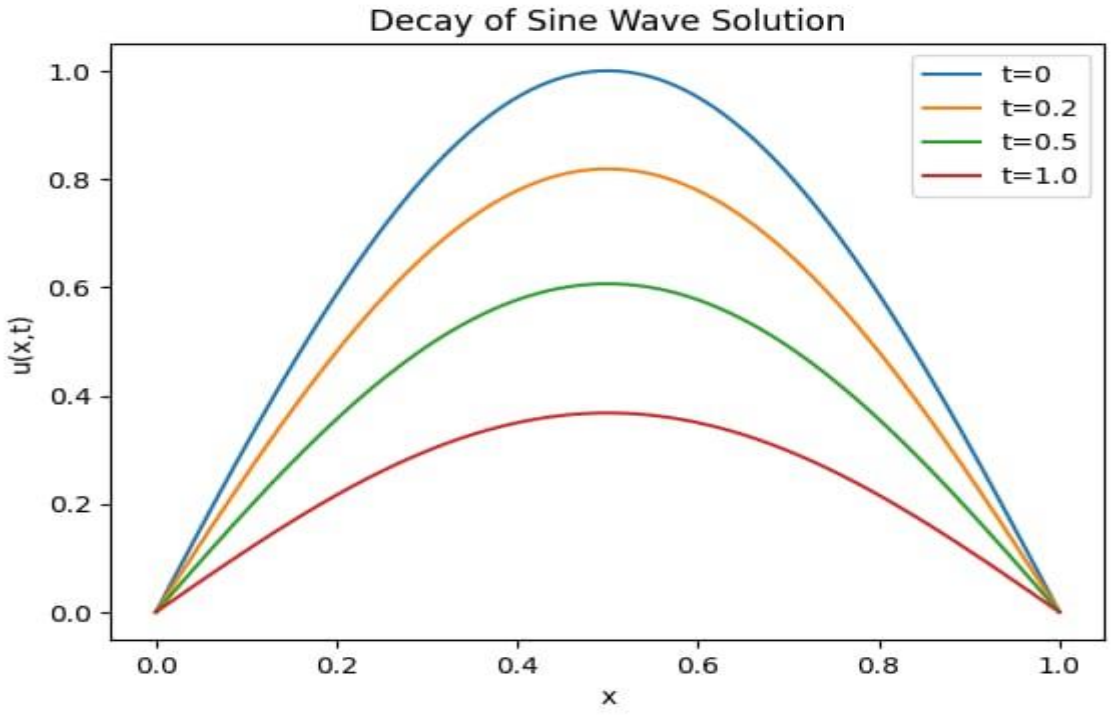

Figure 5. True and numerical solutions for Problem 2 whereas $n=100$, $\alpha=\frac{6}{10}$ and $p\in[-1,1]$.

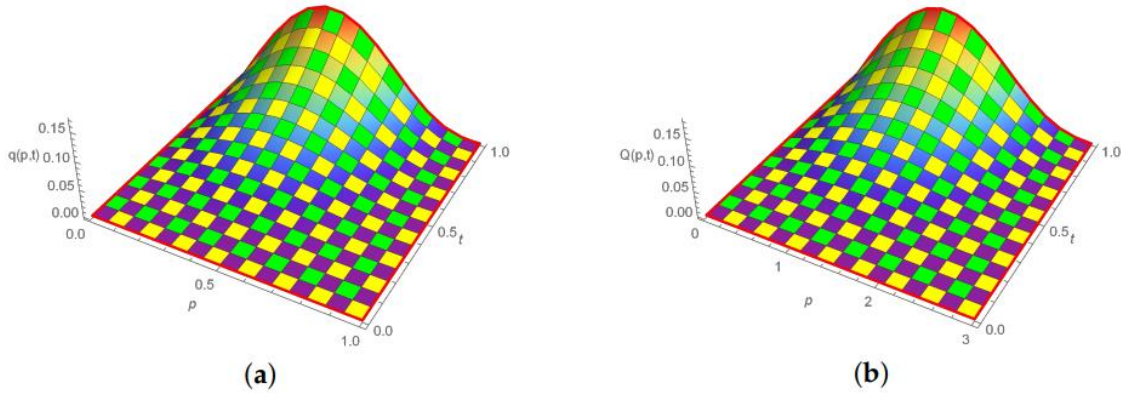

Figure 6. 3D representation of Problem 2, when $n=16$, $\alpha=\frac{8}{10}$, $\Delta t=\frac{1}{1000}$, $t=1$ and $p\in[0,1]$. (a) Exact solution. (b) Numerical solution

Conclusion

In this study, a numerical approach based on the Extended cubic B-spline (ExCBS) method is proposed to solve the Allen–Cahn equation. The ExCBS basis functions are used for spatial discretization, ensuring the smoothness and continuity of the numerical solution, and the finite difference method is used for temporal discretization. The method is shown to be stable and generate accurate numerical solutions with a reasonable spatial and temporal convergence rate.

The scheme is tested with a number of numerical examples. The results reveal that the method is capable of capturing the nonlinear interface evolution and phase transition dynamics of the Allen-Cahn model. Comparisons with other numerical methods suggest that the current method achieves better accuracy and efficiency.

The Extended cubic B-spline method, therefore, provides an accurate and efficient approach for the numerical solution of nonlinear partial differential equations. The method can be applied to more challenging situations such as higher dimensional problems, adaptive grid methods and multiple physical processes. Furthermore, it can be applied to other types of nonlinear evolution equations.

REFRENCES

[1] S. M. Allen and J. W. Cahn, “A microscopic theory for antiphase boundary motion and its application to antiphase domain coarsening,” *Acta Metall.*, vol. 27, no. 6, pp. 1085–1095, 1979.

[2] K. Liu and B. M. Rivière, “Discontinuous Galerkin methods for elliptic partial differential equations with random coefficients,” *Int. J. Comput. Math.*, vol. 90, no. 11, pp. 2477–2490, 2013.

[3] L.-Q. Chen, “Phase-field models for microstructure evolution,” *Annu. Rev. Mater. Res.*, vol. 32, no. 1, pp. 113–140, 2002.

[4] Q. Du and R. A. Nicolaides, “Numerical analysis of a continuum model of phase transition,” *SIAM J. Numer. Anal.*, vol. 28, no. 5, pp. 1310–1322, 1991.

[5] C. De Boor and C. De Boor, *A practical guide to splines*, vol. 27. springer New York, 1978.

[6] M. K. Iqbal, M. Abbas, and N. Khalid, “New cubic B-spline approximation for solving non-linear singular boundary value problems arising in physiology,” *Commun. Math. Appl.*, vol. 9, no. 3, p. 377, 2018.

[7] X. Yang, “Numerical approximations for the Cahn–Hilliard phase field model of the binary fluid-surfactant system,” *J. Sci. Comput.*, vol. 74, no. 3, pp. 1533–1553, 2018.

[8] J. Shen and X. Yang, “Numerical approximations of AllenCahn and Cahn Hilliard equations,” *Discreet. Contin. Dyn. Syst*, vol. 28, no. 4, pp. 1669–1691, 2010.

[9] M. Fatima, R. P. Agarwal, M. Abbas, P. O. Mohammed, M. Shafiq, and N. Chorfi, “Extension of cubic B-spline for solving the time-fractional Allen–Cahn equation in the context of mathematical physics,” *Computation*, vol. 12, no. 3, p. 51, 2024.

[10] D. Hou, Z. Qiao, and L. Ju, “A linear doubly stabilized Crank-Nicolson scheme for the Allen-Cahn equation with a general mobility,” *arXiv Prepr. arXiv2310.19663*, 2023.

[11] B. Rivière, *Discontinuous Galerkin methods for solving elliptic and parabolic equations: theory and implementation*. SIAM, 2008.

[12] T. Journal and O. F. Mathematics, “SOME ENTIRE SOLUTIONS OF THE ALLEN–CAHN EQUATION Yukitaka Fukao, Yoshihisa Morita and Hirokazu Ninomiya,” vol. 8, no. 1, pp. 15–32, 2004.

[13] H. Abboud, C. Al Kosseifi, and J.-P. Chehab, “A stabilized bi-grid method for Allen–Cahn equation in finite elements,” *Comput. Appl. Math.*, vol. 38, no. 2, p. 35, 2019.

[14] M. Shafiq, M. A. Id, H. E. Id, and A. S. M. Alzaidi, “Numerical investigation of the fractional diffusion wave equation with exponential kernel via cubic B-Spline approach,” pp. 1–28, 2023, doi: 10.1371/journal.pone.0295525.

[15] N. Barzehkar, R. Jalilian, and A. Barati, “Hybrid cubic and hyperbolic b-spline collocation methods for solving fractional Painlevé and Bagley-Torvik equations in the Conformable , Caputo and Caputo-Fabrizio fractional derivatives,” vol. 7, 2024, doi: 10.1186/s13661-024-01833-7.

[16] A. S. Heilat, B. Batiha, T. Qawasmeh, and R. Hatamleh, “Hybrid Cubic B-spline Method for Solving A Class of Singular Boundary Value Problems,” vol. 16, no. 2, pp. 751–762, 2023.

[17] X. Yang, J. Zhao, and X. He, "Linear, second order and unconditionally energy stable schemes for the viscous Cahn–Hilliard equation with hyperbolic relaxation using the invariant energy quaternarization method," *J. Comput. Appl. Math.*, vol. 343, pp. 80–97, 2018.

[18] D. Han, A. Brylev, X. Yang, and Z. Tan, "Numerical analysis of second order, fully discrete energy stable schemes for phase field models of two-phase incompressible flows," *J. Sci. Comput.*, vol. 70, no. 3, pp. 965–989, 2017.

[19] M. Shafiq, F. A. Abdullah, M. Abbas, A. Sm Alzaidi, and M. B. Riaz, "Memory effect analysis using piecewise cubic B-spline of time fractional diffusion equation," *Fractals*, vol. 30, no. 08, p. 2240270, 2022.

[20] B. Yin, Y. Liu, H. Li, and S. He, "Fast algorithm based on TT-M FE system for space fractional Allen–Cahn equations with smooth and non-smooth solutions," *J. Comput. Phys.*, vol. 379, pp. 351–372, 2019.

[21] H. Liu, A. Cheng, H. Wang, and J. Zhao, "Time-fractional Allen–Cahn and Cahn–Hilliard phase-field models and their numerical investigation," *Comput. Math. with Appl.*, vol. 76, no. 8, pp. 1876–1892, 2018.

[22] M. G. Sakar, O. Saldır, and F. Erdogan, "An iterative approximation for time-fractional Cahn–Allen equation with reproducing kernel method," *Comput. Appl. Math.*, vol. 37, no. 5, pp. 5951–5964, 2018.

[23] K. Hosseini, A. Bekir, and R. Ansari, "New exact solutions of the conformable time-fractional Cahn–Allen and Cahn–Hilliard equations using the modified Kudryashov method," *Optik (Stuttg).*, vol. 132, pp. 203–209, 2017.

[24] I. Ahmad, M. Saleem, A. Ali, A. Khan, and T. Abdeljawad, "A Computational Analysis of Convection-Diffusion Model with Memory using Caputo-Fabrizio Derivative and Cubic Trigonometric B-Spline Functions," *Eur. J. Pure Appl. Math.*, vol. 18, no. 2, p. 6186, 2025.

[25] A. Mahdav, *Meshfree Methods for Fracture and High-Velocity Impact Simulation*. University of Illinois at Chicago, 2019.

[26] A. Ali, S. Ahmad, I. Hussain, H. Khan, and S. Bushnaq, "Numerical simulation of nonlinear parabolic type Volterra partial integra-differential equations using quartic B-spline collocation method.," *Nonlinear Stud.*, vol. 27, no. 3, 2020.

[27] J. Shen, T. Tang, and L.-L. Wang, "Fourier Spectral Methods for Periodic Problems," in *Spectral Methods: Algorithms, Analysis and Applications*, Springer, 2011, pp. 23–46.

[28] S. Das and S. Tesfamariam, "State-of-the-art review of design of experiments for physics-informed deep learning," *arXiv Prepr. arXiv2202.06416*, 2022.

[29] N. H. F. Beebe, "A Complete Bibliography of Publications in Numriches Mathematik (2000–2009)," 2023.

[30] X. Feng, X. Lin, and R. Derynck, "Smad2, Smad3 and Smad4 cooperate with Sp1 to induce p15 Ink4B transcription in response to TGF-β," *EMBO J.*, vol. 19, no. 19, pp. 5178–5193, 2000.

[31] N. Khalid, M. Abbas, M. K. Iqbal, and D. Baleanu, "A numerical investigation of Caputo time fractional Allen–Cahn equation using redefined cubic B-spline functions," *Adv. Differ. Equations*, vol. 2020, no. 1, 2020, doi: 10.1186/s13662-020-02616-x.